30

Non-invasive Localized Heating and Temperature Monitoring based on a Cavity Applicator for Hyperthermia

Yasutoshi Ishihara[1], Naoki Wadamori[1] and Hiroshi Ohwada[2]
[1]Nagaoka University of Technology, [2]Niigata Sangyo University
Japan

1. Introduction

Hyperthermia, which heats cancer tissue to around 43 °C, is an effective therapeutic technique that is used with radiotherapy or carcinostatic procedures. However, the regression mechanism and therapeutic effect on cancer tissue are not always clear when heating is carried out independently. Moreover, some have expressed skepticism about the clinical value of hyperthermia (Perez et al., 1989; 1991). One reason for this is that it is difficult to heat a local region of a living body to the required temperature in clinical experiments. Furthermore, it has been pointed out that it is difficult to perform non-invasive and precise measurements of the temperature change inside a target object. Currently, therefore, the effect of hyperthermia on cancer tissue in a living body cannot be accurately evaluated and analyzed. Thus, unfortunately, it is sometimes concluded that hyperthermia essentially has few therapeutic effects on cancer.

Hence, it is indispensable to develop an integrated system capable of both heating and quantitative temperature monitoring (temperature measurement) under *in-vivo* conditions in order to identify the factor that specifies the heat sensitivity of cancer tissue, to determine the mechanism of thermal necrosis, and to achieve a completely non-invasive cancer treatment.

Previously, various heat therapies have been proposed that apply wave energy from outside the body to selectively and non-invasively treat localized cancers. Some of these non-invasive methods involve the application of heat to object using dipole antennas (Turner, 1999; Wust et al., 2000) or patch antennas (Paulides et al., 2007a; 2007b) with different amplitudes and phases, or high-temperature thermal ablation using focused ultrasound (FUS) (Lynn et al., 1942; Hynynen et al., 2004; McDannold et al., 2006). Clinical experiments utilizing both methods have been conducted and some good results have been obtained. However, in the method that uses an array antenna, the localized heating of a deeper region is difficult as a relatively larger region can be heated due to the limitations of the electromagnetic wavelength, which, in principle, is determined according to the size of the antenna. Another drawback of this method is that a water bolus is required to prevent excess heating at the surface of the human body (Nadobny et al., 2005). On the other hand, it

is difficult to apply the method that uses FUS to internal organs and tissues surrounded by bones due to the limitations of the characteristics of ultrasound.
In order to non-invasively heat a deep region in a human body, we have proposed a heating applicator that uses an electric field distribution generated by a reentrant cylindrical cavity (Fig. 1), which is widely used in microwave devices, such as cavity-based transducers (Tsubono et al., 1977), linear accelerators (Fujisawa 1958), and electron spin resonance (ESR) spectrometers (Giordano et al., 1983). A reentrant cylindrical cavity is a resonator in which inner cylinders (known as reentrant electrodes) are attached to the upper and lower sides of a cylindrical cavity. Since an intensive electric field is produced in the gap between these reentrant electrodes, a standing wave of the electric field distribution is formed in a heating object when it is placed in this gap, allowing a deep region in a living body to be heated effectively.

(a) (b)

Fig. 1. Localized heating applicator based on a reentrant cylindrical cavity for abdominal organs (a), and head and neck (b).

Through numerical and experimental analyses, we have already reported that localized heating is possible with this method (Matsuda et al., 1988; Kato et al., 1989; 2003; Wadamori et al., 2004). Moreover, in order to improve the therapeutic effects for a localized cancer, we attempted to miniaturize the applicator (Ishihara et al., 2007a; 2008a), as well as optimize the size of the applicator by using experimental design methods (Ishihara et al., 2008b). As a result, we found that the electric field distribution generated between the reentrant electrodes can be localized within a spatial region with a diameter of 70–90 mm. However, when the subject of the treatment is a small cancer localized in the head or neck region, a localized region with a diameter of 30–50 mm must be selectively heated; and thus the heating characteristics achieved in the previous studies were still insufficient. To deal with this issue, we proposed rotating the beam-shaped electric field distribution generated by the reentrant cylindrical cavity, and showed that it is possible to produce focused localized heating by concentrating the electric field distribution in the region around the rotating axis (Ishihara et al., 2008c; 2009; Kameyama et al., 2008).
Thus, although investigations for heating systems are ongoing, the development of non-invasive thermometry is progressing slowly. In most cases during hyperthermia, therefore, only a thermocouple or an optical fiber type thermometer has been used to confirm the heating and treatment effect.

Recently, we proposed non-invasive thermometry using magnetic resonance imaging (MRI) (Ishihara et al., 1992; 1995; Kuroda et al., 1996). The internal temperature change in the object was imaged with a measurement error of less than 1 °C by measuring the water proton chemical shift change observed with MRI. This procedure is performed with a therapeutic device using the techniques mentioned above: focused ultrasound (McDannold et al., 2006) and radiofrequency (RF) waves (Gellermann et al., 2006), as an almost standard non-invasive temperature monitoring method during hyperthermia and cancer ablation treatments. However, a large setup and expensive MRI equipment are necessary for monitoring the temperature change.
Therefore, we focused on the changes in the electromagnetic field distribution inside the heating applicator based on a cavity with temperature changes, and proposed a new non-invasive thermometry method using the temperature dependence of the dielectric constant (Ishihara et al., 2007b; 2007c; Ohwada et al., 2009). Using this concept, after measuring the phase information of the electrical field inside a cavity spatially, an image of the temperature change distribution inside a body is reconstructed by applying the computed tomography (CT) algorithm (Gordon et al., 1970; Goitein 1972; Gordon 1974). Accordingly, since it is easy to fuse this temperature monitoring method with a heating applicator based on a cavity resonator, a novel integrated treatment system is achieved that treats cancer effectively while non-invasively monitoring the heating effect.
By a numerical analysis using a three-dimensional finite element method (FEM) and an experiment using the prototype heating applicator, this study demonstrated the possibility of focusing the electric field distribution by rotating the reentrant cylindrical cavity. The results indicated that when the beam-shaped electric field distribution formed in the reentrant gap was rotated, the heated region became more focused as compared to that without rotating the applicator. In addition, the reconstruction algorithm for the temperature change distribution is discussed in this paper and the efficacy of this method is shown by numerical analyses.

2. Localized heating method

2.1 Principle of the heating system with a reentrant cylindrical cavity

The principle of the heating applicator based on a reentrant cylindrical cavity is explained by the schematic diagram shown in Fig. 2. In this applicator, the reentrant electrodes are attached to the upper and lower sides of a cylindrical cavity. The RF power required for heating is supplied by the loop antenna attached to the upper surface of the cavity, and the characteristic electromagnetic field distribution is formed in a cavity resonator. This field distribution can be explained and compared with that of the conventional radio frequency (RF) capacitive heating system that is commonly used in clinics by using Fig. 3.

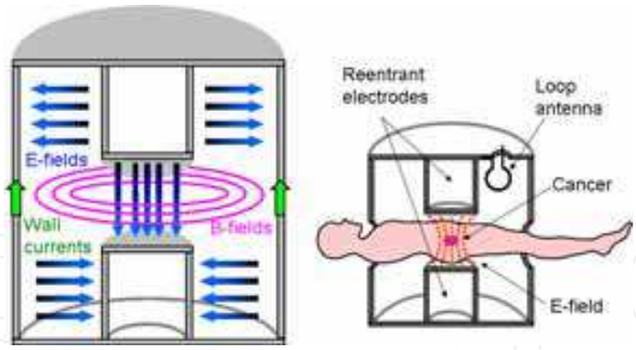

(a) (b)

Fig. 2. Electromagnetic field distribution in a reentrant cylindrical cavity (a), and the setup for a heating target (b).

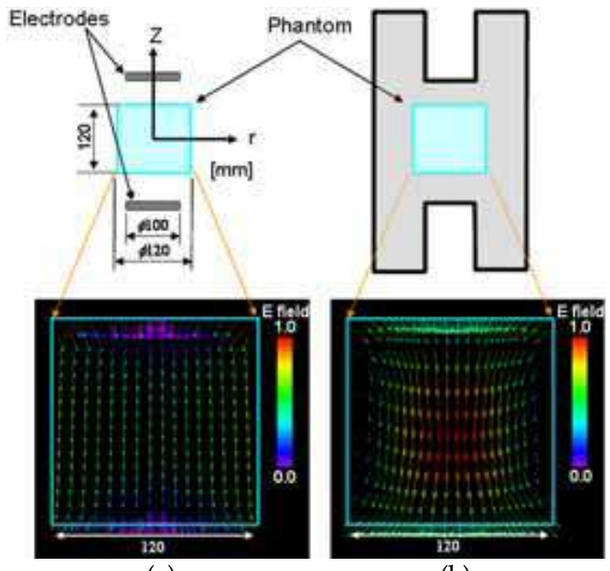

(a) (b)

Fig. 3. Comparison of electric field distributions in a heating object between traditional capacitive heating system (a) and reentrant cylindrical cavity (b).

In an RF capacitive heating system, the electric field distribution is uniform between the electrodes along both the radius (r) and longitudinal (Z) axes; this distribution is expressed by Laplace's equation. Hence, not only the cancer tissue but also the healthy tissues located between the electrodes might become heated. In addition, the electric field tends to concentrate at the ends of the electrodes, and hence the tissues in these areas may be heated excessively; therefore, a water bolus is required to cool the surface of the human body in many cases during treatments. On the other hand, the electromagnetic distribution inside a cavity resonator is expressed by the Helmholtz equation (Eq. (1)). Further, when an electromagnetic distribution is formed inside a reentrant cylindrical cavity resonator with the lowest resonant mode, the electric field distribution is concentrated in the gap between the reentrant electrodes.

$$\begin{aligned} \Delta \boldsymbol{E} + k^2 \boldsymbol{E} &= 0 \\ \Delta \boldsymbol{H} + k^2 \boldsymbol{H} &= 0 \\ k^2 &= \omega^2 \varepsilon \mu \end{aligned} \tag{1}$$

Here, Δ represents the Laplacian; $\boldsymbol{E}$, the electric field vector; $\boldsymbol{H}$, the magnetic field vector; ω, the angular frequency (rad/s); ε, the complex dielectric constant (F/m); and μ, the permeability (H/m). With this heating system, a standing wave will be generated and concentrated between the reentrant electrodes; further, the electric field strength is the highest at the center of the electrode, and decreases rapidly along the r-direction. In addition, since a standing wave of the electric field distribution is also formed in a heating object when it is placed between the reentrant electrodes, the electric field at the midpoint between the electrodes along the Z-direction will also be higher than that closer to the electrodes, unlike RF capacitive heating systems. Thus, by placing a treatment region between the reentrant electrodes for treatment, a deep lesion in a human body can be heated locally, noninvasively, and without contact. By using such a heating system, we confirmed that not only agar phantoms (cubical, oblate spherical, and human-like in shape) but also a dog brain could be heated locally (Kato et al., 2003; Wadamori et al., 2004; Ishihara et al., 2008b).

2.2 Focusing the electric field by rotating the applicator

If the electric field distribution between the reentrant electrodes can be further localized, it will be possible to achieve more localized heating compared to the use of the current applicators. To achieve this, we proposed a method that involves the loading of dielectrics between the reentrant electrodes and a target object, like an electric field absorber (Kroeze et al. 2003), and showed that this method is useful to narrow the electric field distribution and improve the localized heating characteristics, particularly along the r-direction of the applicator (Ishihara et al., 2008d). However, by loading dielectrics, the electric field distribution generated inside a target object became beam-shaped; thus we found that the convergence of the electric field in the Z-direction was more difficult than that in the r-direction due to the formation of this beam-shaped electric field distribution in the Z-direction.

Here, therefore, we propose that the rotation of such a beam-shaped electric field distribution would make it possible to focus the electric field distribution in the region around the rotating axis that is common to the rotating beam-shaped electric field distribution (Ishihara et al., 2008c; 2009; Kameyama et al., 2008). Fig. 4 shows a conceptual schematic image of a rotatable heating applicator.

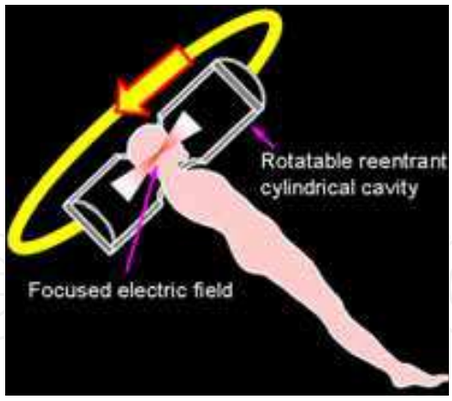

Fig. 4. Concept of a rotatable heating applicator to localize the electric field distribution at the center of a heating target.

3. Non-invasive temperature measurement method

3.1 Measurement of the phase information of the electromagnetic field

Even if non-invasive heating can be achieved, a temperature probe would need to be inserted into the heating target region to measure the temperature change. We therefore considered the temperature dependence of a dielectric constant. For example, the temperature dependence of pure water is given by Eq. (2) (Buckley et al., 1958), allowing the resonant frequency change due to the change in this dielectric constant with temperature to be detected.

$$\varepsilon_r = 87.74 - 0.40\,T + 9.40 \times 10^{-4}\,T^2 - 1.41 \times 10^{-6}\,T^3 \tag{2}$$

Here, T represents a temperature (°C). The dielectric constant of a target material is measured based on the resonant frequency change due to its temperature dependence by using the cavity resonator in the field of material analysis (Pointon et al., 1971; Karikh 1977). However, since it is necessary to measure a frequency change of only tens of kHz, in contrast to a resonant frequency of hundreds of MHz, such a measurement is dramatically difficult when a living body is the target. In such cases, the frequency change with temperature is not measured directly and spatially, but the phase change due to a frequency change may be detected. Thus, the minute frequency change with temperature is detectable as an expanded phase change, that is, $\Delta\theta$, by adjusting the observation time (time delay from when an external electromagnetic wave is applied) for the electromagnetic waves, as expressed in Eq. (3). Accordingly, it is expected that the dynamic range of the detectable temperature change can be improved.

$$\Delta\theta(T(\boldsymbol{r})) \cong 2\pi[f(T(\boldsymbol{r})) - f(T_0(\boldsymbol{r}))]t_{delay} \tag{3}$$

Here, T_0 represents the reference temperature (°C); $\boldsymbol{r}$, the spatial vector; and t_{delay}, the time delays from the reference time (s).

3.2 Introduction of the CT algorithm

Here, electromagnetic waves can be observed only outside the target body. Therefore, it is necessary to estimate the phase change distribution inside a target body and convert this phase change to a temperature change. An example of such an application is the concept that is illustrated in Fig. 5. The phase change distribution of the electromagnetic waves formed between the reentrant gaps is mainly distributed in the direction parallel to an electrical field, which will be shown later. In this case, the projection data reflecting the line integral value of the phase change distribution along the electrical field is similar to the projection data showing X-ray absorption in the case of X-ray CT. Therefore, it is believed that the phase distribution within an object can be estimated by rotating a cavity resonator, in contrast to that obtained in an object with the X-ray CT shown in Fig. 6. We then indicate that the CT algorithm based on the back-projection could be applied by considering the characteristics of the electrical field formed between the reentrant electrodes and the temperature dependence of the dielectrics. In order to evaluate this possibility, a numerical analysis using the finite difference time domain (FDTD) method was carried out and a basic examination of thermometry, which can be easily fused with a heating applicator based on a cavity resonator, was performed.

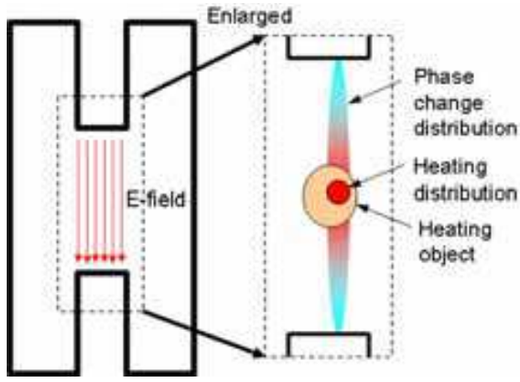

Fig. 5. Phase change distribution before and after the temperature change in a cavity resonator.

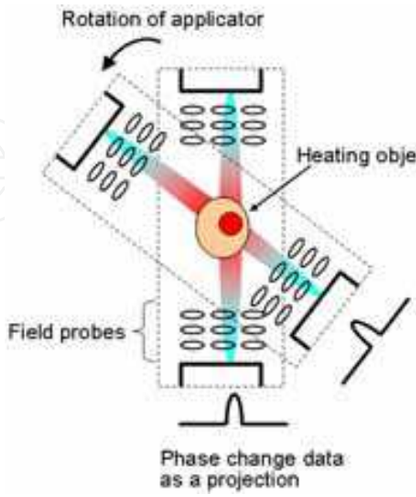

Fig. 6. Reconstruction of a phase change distribution from the projection data by introducing the CT algorithm.

4. Materials and Methods

4.1 Localized heating

4.1.1 Numerical analysis of focused electric field and temperature distributions

To confirm the electric field focusing effect achieved by rotating an applicator, we analyzed the electromagnetic distribution in a reentrant cylindrical cavity model (applicator height: 950 mm, outer diameter: 400 mm, reentrant diameter: 50 mm, and reentrant gap: 350 mm), which is shown in Fig. 7, using a three-dimensional FEM with 15,000 nodes and 1,000 elements. We assumed that the applicator container was an ideal conductor, and an element region corresponding to this assumption was considered to be the perfect electric conductor (PEC) by applying boundary conditions. The size of this model was determined according to our prototype applicator (Ishihara et al., 2009). The target object was a cylindrical phantom with a radius of 160 mm and a height of 160 mm, and we selected a relative permittivity of 63 and an electric conductivity of 0.47 S/m assuming cerebral hyperthermia treatment (Hartsgrove et al., 1987). After the resonant condition inside the cavity was analyzed when the phantom was loaded between the reentrant electrodes, the electromagnetic distribution was calculated.

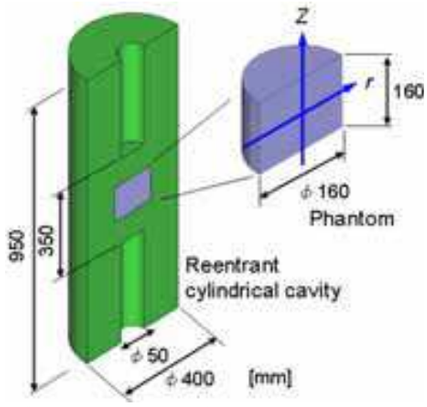

Fig. 7. Numerical heating applicator model with FEM.

The focusing effect of the electric field distribution was evaluated by the full width–half maximum (FWHM) of the normalized SAR distribution along the r- and Z-directions of the phantom inside the applicator.

After obtaining the electromagnetic fields inside the cavity resonator, we calculated the temperature distribution in the phantom based on the coupled analysis of the heating distribution due to the electromagnetic distribution using the three-dimensional FEM with the same model. In this study, it was assumed that the electric field distribution applied to the inside of a phantom did not change at each direction with an applicator's rotation. Then, the SAR distributions formed for each angle of the applicator were overlapped as a heating source, and the temperature distribution was analyzed. The RF power was set up so that the SAR at the center of the phantom became 20 W/kg, and this power was supplied to the phantom from five directions spaced 45 degrees apart with a heating period of 4 minutes for each direction. A comparison with the temperature distribution in the case where the applicator does not rotate (the total heating period was 20 min) was performed. Table 1 showed the values for the thermal parameters of the phantom (Hamada et al., 1998) used in the temperature distribution analysis.

Heat conductivity	[W/m(m K)]	0.55
Specific heat	[J/(kg K)]	4200
Coefficient of heat transfer	[W/(m^3 K)]	20
Volume density	[kg/m^3]	980

Table 1. Heat characteristics of the phantom.

4.1.2 Experimental evaluation of the localized heating effect

To experimentally confirm the focused electric field distribution by rotating a cavity resonator, we developed the prototype system shown in Fig. 8 and performed a phantom experiment. This heating system consists of a reentrant cylindrical cavity, impedance-matching circuit (NCS-04A and NMO1A200M-01; Noda RF Technologies, Suita, Japan), power amplifier (BSA 0125-250; BONN Elektronik, Ottobrunn, Germany), and signal generator (E4430B; Agilent Technologies, Santa Clara, CA, USA). To efficiently transmit the RF power to the cavity resonator, we measured the resonant frequency using a network analyzer (E5061A; Agilent Technologies, Santa Clara, CA, USA), and then the matching circuit was adjusted before the RF power was fed. However, since the matching conditions changed with the rotation of the applicator, the frequency of the applied RF power and the matching conditions at a given angle needed to be re-adjusted with rotation. A cylindrical phantom with a radius of 160 mm and a height of 160 mm (agar: 4%, NaCl: 0.24%, and NaN_3: 0.1%) was fixed on a Teflon table set at the center of the applicator. The electric field strength around the sides of the phantom was measured using an electric field intensity meter (EMR-20; Narda Safety Test Solutions, Pfullingen, Germany); further, the RF power supplied to the applicator was adjusted (20–50 W) so that the SAR value at the center of the phantom was approximately 20 W/kg. To evaluate the heating characteristics, the temperature distribution on a cross-section of the phantom was measured immediately after heating using thermography (TH7102MX; NEC Avio Infrared Technologies, Tokyo, Japan), with a temperature resolution of 0.1 °C and an accuracy of ±0.25 °C.

Fig. 8. Experimental system setup to confirm a focusing effect by rotating an applicator.

4.2 Non-invasive temperature measurement

4.2.1 Numerical model on FDTD

In order to analyze the changes in the transitional electromagnetic field distribution, a three-dimensional FDTD method was used. In this basic examination, the numerical calculation was carried out using a rectangular cavity resonator (1.0 x 1.0 x 1.0 m), since such an

analysis was simple, and the electrical field distribution between the reentrant electrodes in the reentrant cylindrical cavity could be simulated with this rectangular cavity resonator. A cubic solid phantom (0.2 x 0.2 x 0.2 m) was placed in the center of a rectangular cavity resonator, as shown in Fig. 9.

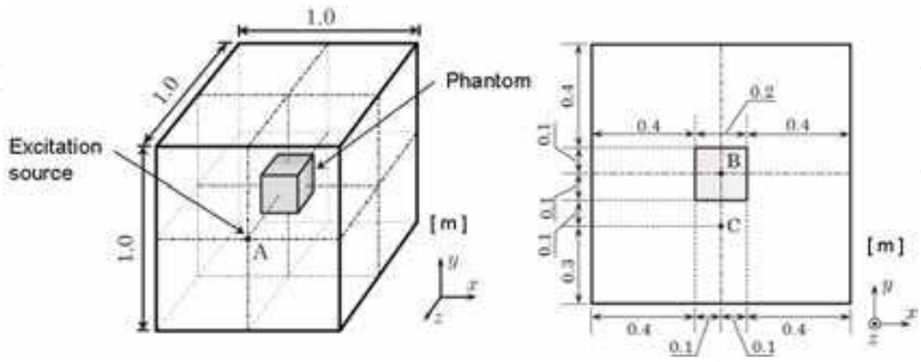

(a) (b)

Fig. 9. Numerical rectangular cavity model for FDTD shown in a perspective diagram (a) and front elevation (b).

In order to increase the analysis accuracy using the FDTD method, the smaller cell size used in this analytic model was preferable, but since the computational resources and computation time required for a simulation become huge when there are a large number of cells, it was necessary to choose an adequate number of cells. Therefore, the resonant frequency estimation error for the number of cells used for the resonator was evaluated in advance, and 95 x 95 x 95 cells were chosen for the abovementioned model, which could achieve a resonant frequency estimate with an error of 0.5% or less. Moreover, the number of cells used for a phantom was set to 19 x 19 x 19. The values shown in Tables 2 and 3 were used as the dielectric constant, conductivity, and permeability for each part. The temperature dependence of the phantom was set to the value of pure water, as shown in Eq. (2).

Parameters	Air	Phantom	Cavity
Permittivity [F/m]	$1.00059\varepsilon_0$	Ref. Table 3	$1.00059\varepsilon_0$
Permeability [H/m]	$1.00000\mu_0$	$0.99999\mu_0$	$0.99998\mu_0$
Electric conductivity [S/m]	0.0000	0.0005	6.1000×10^7

Table 2. Electromagnetic characteristics for FDTD.

Temperature [°C]	Permittivity [F/m]
38.0	$73.81600\varepsilon_0$
43.0	$72.16600\varepsilon_0$

Table 3. Permittivity with temperature of phantom.

Since the electrical field component ***Ez*** parallel to a reentrant electrode (called the TM010 mode) was formed in the abovementioned heating applicator shown in Fig. 2, in order to achieve an equivalent electric field distribution in a rectangular cavity resonator, the excitation source expressed with Eq. (4) was used. By applying this exciting pulse, the

electric field distribution ***Ey*** was formed in the perpendicular direction of a rectangular cavity resonator (called the TE101 mode). Then, the phase change distribution on the x-y plane parallel to an electric field vector was observed.

$$H_x(t) = A \exp\{-[(t - T_B)/0.29T_B]^2\} \sin(2\pi f_0 t) \quad (4)$$

Here, $T_B = 0.646/f_B$, f_B represents the excitation frequency band (Hz), A is the amplitude of the excitation pulse, and f_0 is the resonant frequency (Hz).

4.2.2 Numerical analysis of the phase change distribution

The phase change distribution with temperature (38–43 °C) was computed. In this study, the time delay from the reference time was set at around 200 ns, which provided a high sensitivity for detecting a phase change with temperature.

In order to estimate the temperature distribution inside a phantom using just the phase distribution of the external region, projection data for 32 directions were prepared from the phase distributions calculated for the rectangular cavity resonator, which rotated in 11.25 degree steps. The projection data for each column were determined as integrated values of the phase change along a projection direction (y-direction) within the line integral range shown in Fig. 10; however, the phase changes within the phantom region were not integrated into the projection data. The phase change distributions inside a phantom with temperature changes were reconstructed by a simple back projection and a filtered back projection with a Shepp-Logan filter (Shepp et al., 1974).

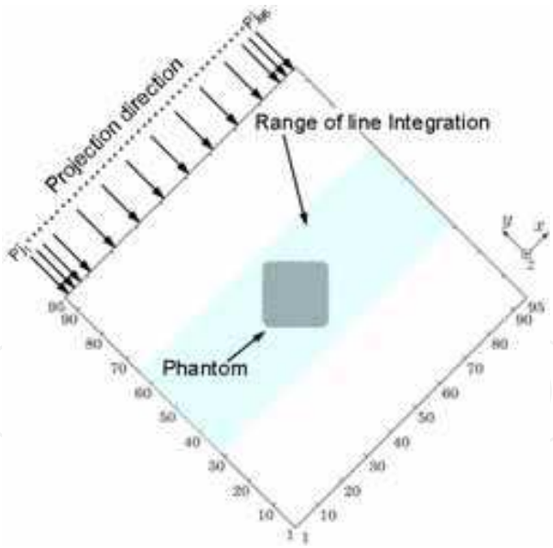

Fig. 10. Integration region to determine projection data (in a case where the applicator angle was 45°).

5. Results and discussion

5.1 Localized heating effect by rotating the applicator

The results of electromagnetic field and modal analyses showed that the electromagnetic field distribution in the reentrant cylindrical resonator shown in Fig. 11 had a resonant frequency of 226.5 MHz. Fig. 12 shows the normalized SAR distributions at the central plane (r–Z plane) of the phantom. The FWHM in the r and Z directions were 60.0 mm and 101.2 mm, respectively. When considering the normalized SAR distribution in the Z-direction, the convergence of the electric field in the Z-direction is more difficult than that in the r-direction without rotating the applicator.

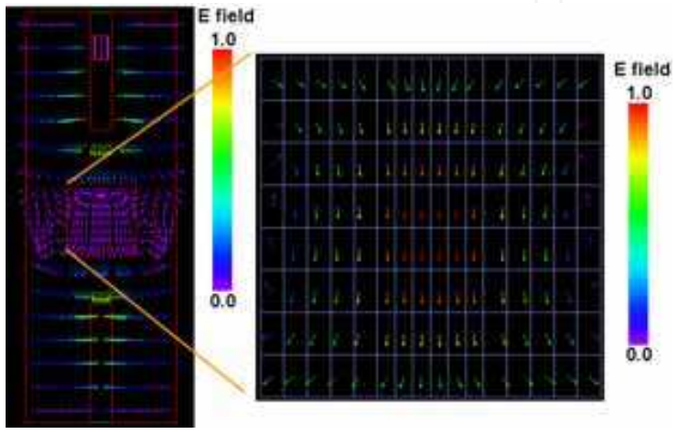

(a) (b)

Fig. 11. Numerically simulated electric field distribution inside an applicator (a), and a phantom (b).

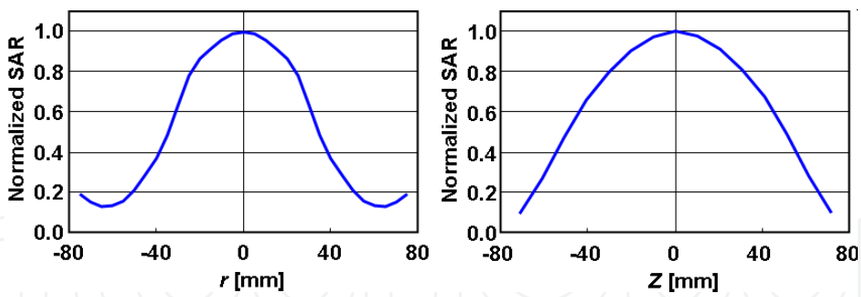

(a) (b)

Fig. 12. Normalized SAR distribution in the r (a) and Z (b) directions.

Therefore, we evaluated the focusing effect by rotating the beam-shaped electric field distribution, and showed the temperature distribution of a cross-section (r–Z plane) at the center of the agar phantom with and without rotation of the applicator, as shown in Fig. 13. We evaluated the heating region by the FWHM of the temperature distribution and confirmed that the localized heating region could be improved by approximately 16% by rotating in the Z-direction; the FWHM was 107.1 mm without rotating the applicator, while it was 92.5 mm when the applicator was rotated (Fig. 14).

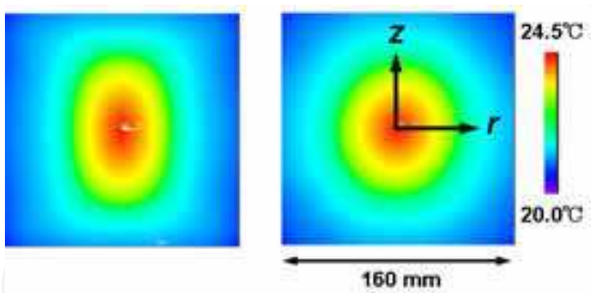

(a) (b)

Fig. 13. Temperature distributions of a cross-section at the center of the phantom without rotation (a) and with rotation (b).

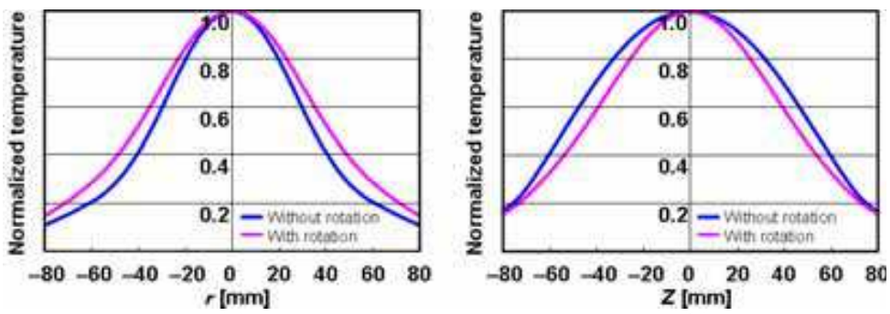

(a) (b)

Fig. 14. Temperature profile along the r (a) and Z (b) directions normalized with the maximum temperature corresponding to that shown in Fig. 13.

In addition, Fig. 15 shows an example of a fundamental experiment to confirm the possibility of focusing the electric field distribution by rotating the applicator. These temperature distributions show a cross-section (r–Z surface) at the center of the agar phantom with and without rotation of the applicator with an incident RF power of approximately 25 W, which corresponds to an SAR of 20 W/kg at the object center and a total heating period of 20 min. Fig. 16 shows the temperature distribution along the r and Z directions. These figures indicate that the results of the numerical analysis and those obtained in the experiment were almost identical. From these experimental results, we evaluated the heating region by the FWHM of the temperature distribution and confirmed that the localized heating region could be improved by approximately 21% by rotating an applicator in the Z-direction; the FWHM was 101.2 mm without rotation, while it was 83.7 mm when the applicator was rotated.

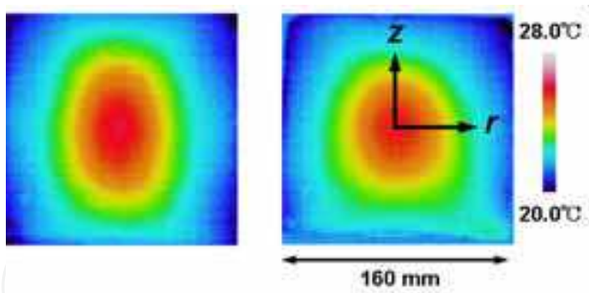

(a) (b)

Fig. 15. Temperature distributions of a cross-section at the center of the phantom without rotation (a) and with rotation (b).

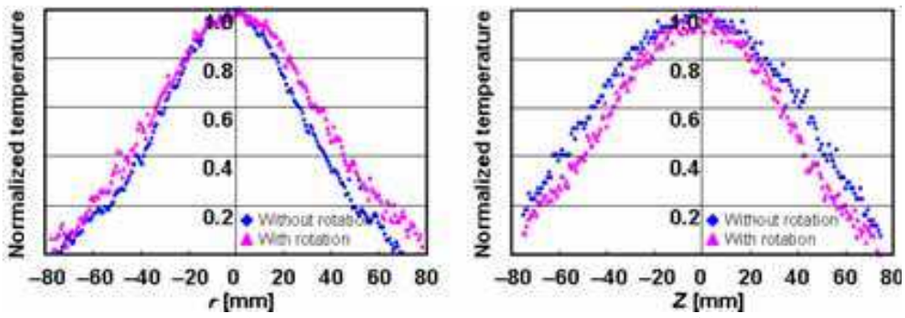

(a) (b)

Fig. 16. Temperature profile along the r (a) and Z (b) directions normalized with the maximum temperature corresponding to that shown in Fig. 15.

These results indicated that the heating region was focused in the Z-direction, although the narrowing effect degrades in the r-direction due to the averaging of the electric fields by the rotation of the heating region. One idea is to focus such a narrowed electric field distribution in the Z-direction after narrowing the electric field distribution in the r-direction by loading dielectrics (Ishihara et al., 2008d). In addition to this complementary procedure, miniaturizing the diameter of the reentrant electrodes is another potential way to greatly improve the localized heating characteristics. However, since the narrowing effect of the electric field in the r-direction and the concentration effect of the electric field in the Z-direction have a trade-off relationship, it is necessary to optimize these parameters, taking into consideration the rotation of the applicator.
By using the abovementioned methods and optimizing both the size and rotation conditions of the heating applicator, we could predict that the localized heating region would be an area with a diameter of 50–60 mm.

5.2 Noninvasive temperature measurement

When a temperature change of 5 °C (from 38 to 43 °C) was generated in the phantom, there was a phase change in the electric field formed in the rectangular cavity resonator (t_{dealy} = 200 ns), as indicated in Fig. 17. According to this figure, the phase change with temperature was produced mainly as a distribution along the electrical field direction (y-direction in Fig. 18(b)), corresponding to the region at which the temperature change was produced

compared with the direction (x-direction in Fig. 18(a)) perpendicular to the electric field. It was confirmed that such behavior for an approximate distribution did not change when the applied field direction was changed by rotating the cavity resonator, as shown in Fig. 19. Then the phase projection data in the direction of the electrical field were computed according to the line integral, as in the X-ray CT mentioned above, and the phase change distribution within the target object was estimated.

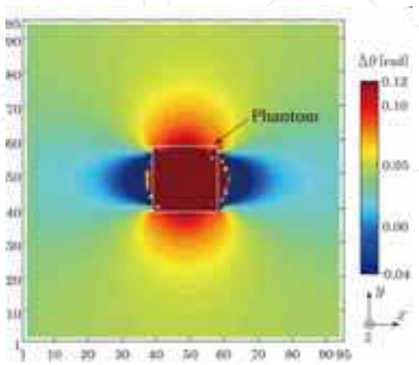

Fig. 17. Phase change distribution with temperature change from 38 to 43 °C at the center of the x-y plane.

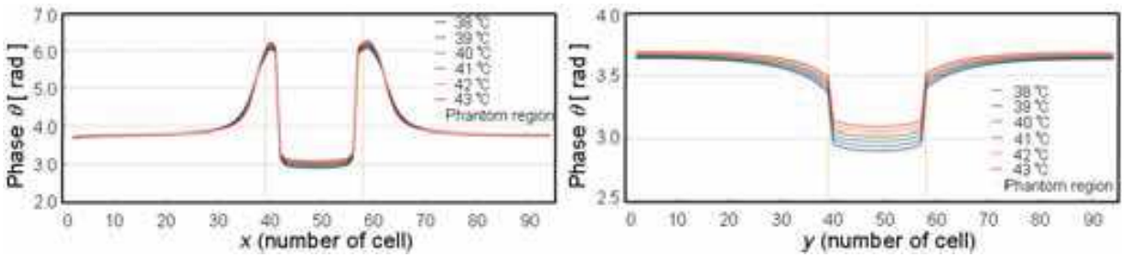

(a) (b)

Fig. 18. Phase change distribution with temperature change from 38 to 43 °C along the x (a) and y (b) directions on the center x-y plane.

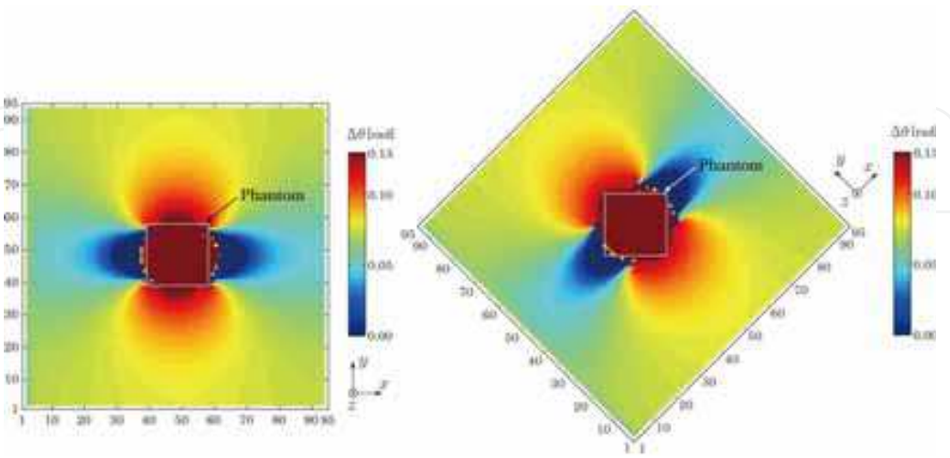

(a) (b)

Fig. 19. Phase change distribution with temperature change from 38 to 43 °C at the rotation angles of 0 degree (a) and 45 degrees (b) at the center of the x-y plane.

Fig. 20 shows the reconstructed phase change distributions with a simple back-projection CT algorithm when the number of projections was 32. As anticipated, the surroundings of the reconstructed phase change distribution were blurred due to the point spread function of the simple back-projection. Therefore, in order to compensate for such broadening of the phase distribution, a filtered back projection with a Shepp-Logan filter was applied to the projection data (Fig. 21). As a result of this filtering, the reconstruction error due to image blurring was reduced by approximately 60%. Although degradation of the spatial resolution resulting from the broadening of the phase distribution was mentioned as a problem under the current circumstances, and an evaluation of the thermometry accuracy was difficult due to the still large image blurring, it was shown that the detection of a 1 °C temperature change, which is required of hyperthermia (Delannoy et al., 1991), can be sufficiently measured by the phase change with temperature. However, since it is expected that the temperature dependence of a dielectric constant changes with tissues (Jaspard et al., 2002), for clinical application it will be necessary to devise a method to convert from a phase value to temperature and to evaluate the measurement error generated in the required temperature range.

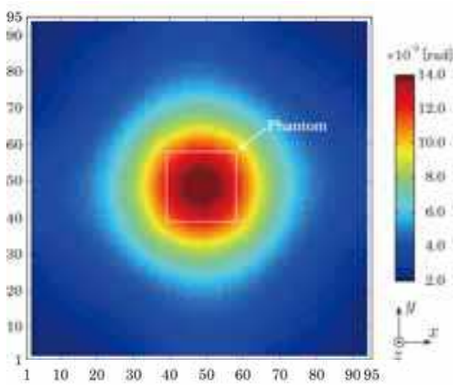

Fig. 20. Reconstructed phase change distribution with a simple back projection.

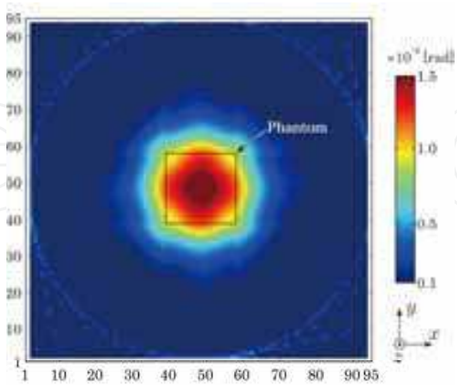

Fig. 21. Reconstructed phase change distribution with a Shepp-Logan filter.

In addition, the reconstruction error regarding the detected position was evaluated when the measurement subject was shifted from the center position of the cavity resonator. Fig. 22 shows the reconstructed results with the simple back projection and filtered back projection

methods, respectively. When the shifted distance of a phantom was set at 4.21 cm (which corresponded to 4 cells of the FDTD numerical model), the detected distance from the reconstructed phase distribution with a simple back-projection was 5.15 cm, which corresponded to a relative error of 23.3% compared to the true value. In contrast, the detected distance from the reconstructed phase distribution with a filtered-back-projection was 4.69 cm, which corresponded to a relative error of 11.3%. Consequently, it became clear that the position of a heating region was detectable with this method, with an accuracy corresponding to a spatial resolution of one or less cell. Conversely, since this detection accuracy may be restrained by the size of the cell used with this FDTD, it is necessary to investigate spatial resolution while including other factors in the future.

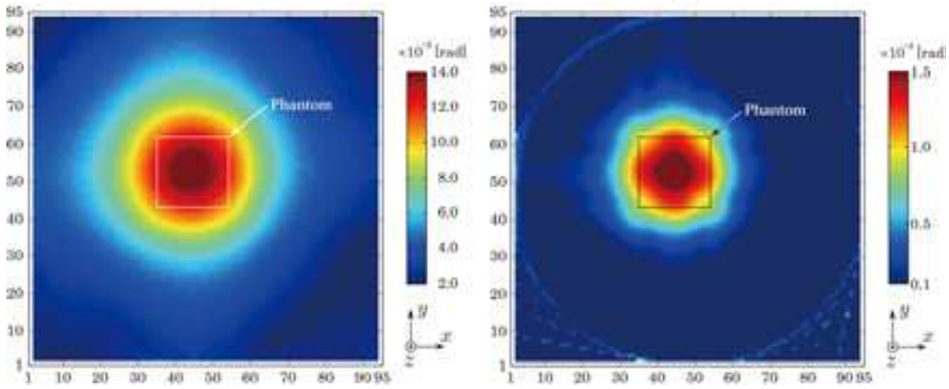

(a) (b)

Fig. 22. Reconstructed phase change distributions by a simple back projection (a) and filtered back projection (b) when the phantom position was shifted from the center of the cavity resonator.

6. Conclusions and Future Research

A heating region with a diameter of approximately 85–90 mm was obtained by rotating a beam-shaped electric field distribution. This corresponded to an improvement in the heating region of 15–20%, compared to a case in which heating was carried out without rotating the applicator. Although this is insufficient to heat a cancer localized in the head or neck region, such a heating method has the potential of achieving a heating region with a diameter of less than 50 mm by optimizing the beam-shaped electric field distribution and rotation conditions. However, further improvement in the localized characteristics may be difficult due to the restrictions of the trade-off between the convergence of electric fields in the r and Z-directions.

On the other hand, it is possible to achieve more localized heating by noninvasive real-time temperature measurement and active temperature control since the heat source generated by the heating applicator based on a reentrant cylindrical cavity indicates an approximately concentrated spherical distribution whose intensity is maximum at the center of the heating target body. Since the proposed method to measure temperature distribution from the information on the electromagnetic waves inside a cavity resonator can be easily embedded in our heating applicator, a novel cancer treatment system that combines the localized heating of cancer with non-invasive temperature monitoring can be established.

Consequently, a cancer treatment for a lesion with a diameter of approximately 30–50 mm, which is required to heat a cancer localized in the head or neck region, can be achieved.

7. Acknowledgement

This study was supported by the Industrial Technology Research Grant Program 2006 from the New Energy and Industrial Technology Development Organization (NEDO) of Japan, and a Grant–in–Aid for Scientific Research (B), 20300155, 2008 from the Japan Society for the Promotion of Science (JSPS).

8. References

Buckley, F. & Maryott, A. A. (1958). Tables of Dielectric Dispersion Data for Pure Liquids and Dilute Solutions. *Natl. Bur. Stand. Circ.* 589, US Government Printing Office, 10–18353, Washington, DC

Delannoy, J.; Chen, C., Turner, T., Levin, R. L. & Le Bihan, D. (1991). Noninvasive temperature imaging using diffusion MRI. *Magn. Reson. Med.*, Vol. 19, No.2, Jun. 1991, 333–339, 0740–3194

Fujisawa, K. (1958). General treatment of klystron resonant cavities. *IRE Trans. Microwave Theory and Tech.*, Vol. 6, No. 4, Oct. 1958, 344–358, 0097–2002

Gellermann, J.; Wlodarczyk, W., Hildebrandt, B., Ganter, H., Nicolau, A., Rau, B., Tilly, W., Fähling, H., Nadobny, J., Felix, R. & Wust, P. (2006). Noninvasive magnetic resonance thermography of recurrent rectal carcinoma in a 1.5 tesla hybrid system. *Cancer Res.*, Vol. 63, No. 13, Jul. 2005, 5872–5880, 0008–5472

Giordano, M.; Momo, F. & Sotgiu, A. (1983). On the design of a re-entrant square cavity as resonator for low-frequency ESR spectroscopy. *J. Phys. E: Sci. Instrum.*, Vol. 16, No. 8, Aug. 1983, 774–779, 0022–3735

Goitein, M. (1972). Three-dimensional density reconstruction from a series of two-dimensional projections. *Nuclear Instruments and Methods*, Vol. 101, No. 3, Jun, 1972, 509–518, 0168–9002

Gordon, R.; Bender, R. & Herman, G. T. (1970). Algebraic reconstruction techniques (ART) for three-dimensional electron microscopy and X-ray photography. *J. Theor. Biol.*, Vol. 29, No. 3, Dec. 1970, 471–481, 0022–5193

Gordon, R. (1974). A tutorial on ART. *IEEE Trans. Nucl. Sci.*, Vol. NS-21, No. 3, Jun. 1974, 78–93, 0018–9499

Hamada, L.; Furuya, K. & Ito, K. (1998). Biological tissue-equivalent phantom for microwave hyperthermia. *Jpn. J. Hyperthermic Oncol.*, Vol. 14, No. 1, Mar. 1998, 31–40, 0197–8462, 0911–2529 (Japanese)

Hartsgrove, G.; Kraszewski, A. & Surowiec, A. (1987). Simulated biological materials for electromagnetic radiation absorption studies. *Bioelectromag*, Vol. 8, No. 1, Jan. 1987, 29–36, 0197–8462

Hynynen, K.; Clement, G. T., McDannold, N., Vykhodtseva, N., King, R., White, P. J., Vitek, S. & Jolesz, J. (2004). 500-element ultrasound phased array system for noninvasive focal surgery of the brain: a preliminary rabbit study with ex vivo human skulls. *Magn. Reson. Med.*, Vol. 52, No. 1, Jul. 2004, 100–107, 0740–3194

Ishihara, Y.; Calderon, A., Watanabe, H., Mori, K., Okamoto, K., Suzuki, Y., Sato, K., Kuroda, K., Nakagawa, N. & Tsutsumi, S. (1992). A precise and fast temperature mapping using water proton chemical shift, *Proceedings of Society of Magnetic Resonance in Medicine, 11th Annual Meeting*, pp. 4804, Berlin, Germany, Aug. 1992

Ishihara, Y.; Calderon, A., Watanabe, H., Okamoto, K., Suzuki, Y., Kuroda, K. & Suzuki, Y. (1995). A precise and fast temperature mapping using water proton chemical shift. *Magn. Reson. Med.*, Vol. 34, No. 6, Dec. 1995, 814–823, 0740–3194

Ishihara, Y.; Gotanda, Y., Wadamori, N. & Matsuda, J. (2007a). Hyperthermia applicator based on reentrant cavity for localized head and neck tumors. *Rev. Sci. Inst.*, Vol. 72, No. 2, Feb. 2007, 024301.1–024301.8, 0034–6748

Ishihara, Y.; Endo, Y. Wadamori, N. & Ohwada, H. (2007b). A noninvasive temperature measurement regarding the heating applicator based on a reentrant cavity, *Proceedings of 2007 Joint Annual Meeting of the. World Conference on Interventional. Oncology (WCIO) and the Society for. Thermal Medicine (STM)*, pp. 232–233, Washington, DC, USA, May 2007

Ishihara, Y.; Endo, Y., Ohwada, H. & Wadamori, N. (2007c). Noninvasive thermometry in a reentrant resonant cavity applicator, *Proceedings of the IEEE of the 29th Annual International Conference of the Engineering in Medicine and Biology Society, 2007*, pp. 1487–1490, Lyon, France, Aug. 2007

Ishihara, Y. & Wadamori, N. (2008a). Localized heating characteristics of hyperthermia using a reentrant cavity. *J Med Eng*, Vol. 32, No. 5, Sep. 2008, 348–357, 0309–1902

Ishihara, Y. & Wadamori, N. (2008b). Heating applicator based on reentrant cavity with optimized local heating characteristics. *Int. J. Hyperthermia*, Vol. 24, No. 8, Dec. 2008, 694–704, 0265–6736

Ishihara, Y. & Wadamori, N. (2008c). Improvement in the localized heating characteristics by the rotation of a heating applicator based on a reentrant cavity, *Proceedings of 10th International Congress on Hyperthermic Oncology*, pp. 1487, Munich, Germany, Apr. 2008

Ishihara, Y.; Kameyama, Y., Ino, Y. & Wadamori, N. (2008d). Improvement in localized heating characteristics by loading dielectrics in a heating applicator based on a cylindrical reentrant cavity. *Thermal Med.*, Vol. 24, No. 2, Aug. 2008, 61–72, 1882–2576

Ishihara, Y.; Kameyama, Y. & Wadamori, N. (2009). Localized heating method by a rotatable applicator based on a reentrant cylindrical cavity, *Proceedings of Society for Thermal Medicine 2009 Annual Meeting*, pp. 172, Tucson, AZ, USA, Apr. 2009

Jaspard, F. & Nadi, M. (2002). Dielectric properties of blood: an investigation of temperature dependence. *Physiol. Meas.*, Vol. 23, No. 3, Aug. 2002, 547–554, 0967–3334

Kameyama, Y. & Ishihara, Y. (2008). Regional heating by insertion of dielectrics and rotation of the focused electric field in the hyperthermia, *Proceedings of the IEEE of the 30th Annual International Conference of the Engineering in Medicine and Biology Society, 2008*, pp. 4380–4383, Vancouver, Canada, Aug. 2008

Karikh, N. M. (1977). Method of calculating dielectric permittivity in a partly filled resonator cavity. Measurement Techniques, Vol. 20, No. 5, May 1977, 68–71, 0543–1972

Kato, K.; Matsuda, J. & Saitoh, Y. (1989). A re-entrant type resonant cavity applicator for deep-seated hyperthermia treatment, *Proceedings of the Annual International Conference of the IEEE Engineering in Medicine and Biology Society, 1989*, pp. 1712–1713, Seattle, WA, USA, Nov. 1989

Kato, K.; Wadamori, N., Matsuda, J., Uzuka, T., Takahashi, H. & Tanaka, R. (2003). Improvement of the resonant cavity applicator for brain tumor hyperthermia, *Proceedings of the IEEE of the 25th Annual International Conference of the Engineering in Medicine and Biology Society, 2003*, pp. 3271–3274, Cancun, Mexico, Sep. 2003

Kroeze, H.; Van Vulpen M., De Leeuw, A. A. C., De Kamer, J. B. & Lagendijk, J. J. W. (2003). Improvement of absorbing structures used in regional hyperthermia. Int. J. Hyperthermia, Vol. 19, No. 6, Nov. 2003, 598–616, 0265–6736

Kuroda, K.; Suzuki, Y., Ishihara, Y. Okamoto, K. & Suzuki, Y. (1996). Temperature mapping by water proton chemical shift obtained with 3D-MRSI -Feasibility in vivo-. *Magn. Reson. Med.*, Vol. 35, No. 1, Jan. 1996, 20–29, 0740–3194

Lynn, J. G.; Zwemer, R. L., Chick, A. J. & Miller, A. E. (1942). A new method for the generation and use of focused ultrasound in experimental biology. *J. Gen. Physiol.*, Vol. 26, No. 2, Nov. 1942, 179–193, 0022–1295

Matsuda, J.; Kato, K. & Saitoh, Y. (1988). The application of a re-entrant type resonant cavity applicator to deep and concentrated hyperthermia. *Jpn. J. Hyperthermia Oncol.*, Vol. 4, No. 2, Jun. 1988, 111–118, 0911–2529 (in Japanese)

McDannold, N.; Tempany, C. M., Fennessy, F. M., So, M. M., Rybicki, F. J., Stewart, E. A., Jolesz, F. A. & Hynynen, K. (2006). Uterine leiomyomas: MR imaging-based thermometry and thermal dosimetry during focused ultrasound thermal ablation. *Radiology*, Vol. 240, No. 1, Jul. 2006, 263–272, 0033–8419

Nadobny, J.; Wlodarczyk, W., Westhoff, L., Gellermann, J., Felix, R. & Wust, P. (2005). A clinical water-coated antenna applicator for MR-controlled deep-body hyperthermia: a comparison of calculated and measured 3-D temperature data sets. *IEEE Trans. Biomed. Eng.*, Vol. 52, No. 3, Mar. 2005, 505–519, 0018–9294

Ohwada, H. & Ishihara, Y. (2009). Noninvasive thermometry on the heating applicator based on the reentrant cavity. *The IEICE transactions on information and systems (Japanese edition)*, Vol. 92-D, No. 4, Apr. 2009, 562–570, 1880–4535 (in Japanese)

Paulides, M. M.; Bakker, J. F., Zwamborn, A. P. M. & Van Rhoon, G. C. (2007a). A head and neck hyperthermia applicator: Theoretical antenna array design. *Int. J. Hyperthermia*, Vol. 23, No. 1, Feb. 2007, 59–67, 1464–5157

Paulides, M. M.; Bakker, J. F., Neufeld, E., Van Der Zee, J., Jansen, P. P., Levendag, P. C. & Van Rhoon, G. C. (2007b). The HYPERcollar: A novel applicator for hyperthermia in the head and neck. *Int. J. Hyperthermia*, Vol. 23, No. 7, Nov. 2007, 567–576, 1464–5157

Perez, C. A.; Gillespie, B., Pajak, T., Emami, N. B. & Rubin, P. (1989). Quality assurance problems in clinical hyperthermia and their impact on therapeutic outcome: a report by the Radiation Therapy Oncology Group. *Int. J. Radiat. Oncol. Biol. Phys.*, Vol. 16, No. 3, Mar. 1989, 551–558, 0360–3016

Perez, C. A.; Pajak, T., Emami, B., Hornback, N. B., Tupchong, L. & Rubin, P. (1991). Randomized phase III study comparing irradiation and hyperthermia with irradiation alone in superficial measurable tumors. Final report by the Radiation Therapy Oncology Group. *Am. J. Clin. Oncol.*, Vol. 14, No. 2, Apr. 1991, 133–141, 0277–3732

Pointon, A. J. & Woodman, K. F. (1971). A coaxial cavity for measuring the dielectric properties of high permittivity materials. *J. Phys. E: Sci. Instrum.*, Vol. 4, No. 3, Mar. 1971, 208–210, 0022–3735

Shepp, L. A. & Logan, B. F. (1974). The Fourier reconstruction of a head section. *IEEE Trans. Nucl. Sci.*, Vol. NS-21, No. 3, Jun. 1974, 21–43, 0018–9499

Tsubono, K.; Hiramatsu, S. & Hirakawa, H. (1977). Cavity transducer for subatomic mechanical vibration. *Jpn. J. Appl. Phys.*, Vol. 16, No. 9, Sep. 1977, 1641–1645, 0021–4922

Turner, P. F. (1999). MRI integration with 3D phased array BSD–2000 3D hyperthermia system, *Proceedings of the 1st Joint BMES/EMBS Conference*, pp. 1278, Atlanta, GA, USA, Oct. 1999

Wadamori, N.; Matsuda, J., Takahashi, H., Grinev, I., Uzuka, T. & Tanaka, R. (2004). Heating properties of a re-entrant cavity-type applicator for deep regional hyperthermia treatments, *Proceedings of 9th International Congress on Hyperthermic Oncology*, pp. 169, St. Louis, MO, USA, Apr. 2004

Wust, P.; Beck, R., Berger, J., Seebass, M., Wlodarczyk, W., Hoffmann, W. & Nadobny, J. (2000). Electric field distributions in a phased–array applicator with 12 channels: Measurements and numerical simulations. *Med. Phys.*, Vol. 17, No. 11, Nov. 2000, 2565–2579, 0094–2405

IntechOpen

New Developments in Biomedical Engineering
Edited by Domenico Campolo

ISBN 978-953-7619-57-2
Hard cover, 714 pages
Publisher InTech
Published online 01, January, 2010
Published in print edition January, 2010

Biomedical Engineering is a highly interdisciplinary and well established discipline spanning across engineering, medicine and biology. A single definition of Biomedical Engineering is hardly unanimously accepted but it is often easier to identify what activities are included in it. This volume collects works on recent advances in Biomedical Engineering and provides a bird-view on a very broad field, ranging from purely theoretical frameworks to clinical applications and from diagnosis to treatment.

How to reference
In order to correctly reference this scholarly work, feel free to copy and paste the following:

Yasutoshi Ishihara, Naoki Wadamori and Hiroshi Ohwada (2010). Non-invasive Localized Heating and Temperature Monitoring based on a Cavity Applicator for Hyperthermia, New Developments in Biomedical Engineering, Domenico Campolo (Ed.), ISBN: 978-953-7619-57-2, InTech, Available from: http://www.intechopen.com/books/new-developments-in-biomedical-engineering/non-invasive-localized-heating-and-temperature-monitoring-based-on-a-cavity-applicator-for-hyperther

INTECH
open science | open minds

InTech Europe
University Campus STeP Ri
Slavka Krautzeka 83/A
51000 Rijeka, Croatia
Phone: +385 (51) 770 447
Fax: +385 (51) 686 166
www.intechopen.com

InTech China
Unit 405, Office Block, Hotel Equatorial Shanghai
No.65, Yan An Road (West), Shanghai, 200040, China
中国上海市延安西路65号上海国际贵都大饭店办公楼405单元
Phone: +86-21-62489820
Fax: +86-21-62489821

IntechOpen